Supporting Information

Electronic Nature of Linkers Based Conjugated Microporous Polymers: A Sustainable Approach to Enhance CO_2 Capture

Mohammed G. Kotp, Ahmed F. M. EL-Mahdy,* Mitch Ming-Chi Chou, and Shiao-Wei Kuo*

Department of Materials and Optoelectronic Science, Center of Crystal Research, National Sun Yat-Sen University, Kaohsiung, 80424, Taiwan

Corresponding Author:

E-mail: ahmedelmahdy@mail.nsysu.edu.tw (A. F. M. EL-Mahdy), and

kuosw@faculty.nsysu.edu.tw (S. W. Kuo)

S1 Instrumentation

S.1.1 Fourier transform infrared (FTIR) scans.

Classical KBr plates were exploited for FTIR sweeps through a 27 Bruker Tensor spectrophotometer. Resolution scales were modulated by 4 cm^{-1}.

S.1.2 ^{1}H and ^{13}C NMR scans.

NMR profiles were swept through An INOVA 500 machine employing DMSO-d_6 as well as $CDCl_3$ as solvents, in addition to employing Tetramethylsilane (TMS) as external standard. Chemical shifts are shown in part per million (ppm).

S.1.3 Thermal gravimetric analysis (TGA).

TGA of CMPs were provided under N_2 stream using TA Q-50 instrument. A closed Pt cane was used as sample holder, after that temperature was raised up to 800 °C under ramp of 20 °C min^{-1} at N_2 stream of an average of 50 ml min^{-1}.

S.1.4 Solid state nuclear magnetic resonance (SSNMR).

The Bruker Avance 400 NMR detector connected to the probe of Bruker magic-angle-spinning (MAS) was employed for recording SSNMR profiles at a running of 32,000 scans.

S.1.5 Surface area, and porous features.

Micromeritics ASAP 2020 surface area as well as porosity analyzer were employed for evaluating surface area and porosimetry of every CMP. Ultrapure N_2 stream (up to ca. 1 atm) as well as a liquified N_2 bath extremely facilitated the obtaining of nitrogenic isotherms.

S.1.6 X-ray photoelectron spectroscopy (XPS) spectra.

Thermo Fisher scientific ESCALAB 250 connected a micro monochromatic Al Kα X-ray lamp (15 kV) with a dual-focusing full 180° spherical sector electron analyzer determined XPS scans.

S.1.7 Field-emission scanning electron microscopy (FE-SEM).

A JEOL JSM-7610F of SEM used for visualizing FE-SEM images. Notably, CMPs were sputtered using Pt for 150 s for clear visualization.

S.1.8 Transmission electron microscopy (TEM).

TEM visualizations of the obtained CMPs were checked through a JEOL-2100 scanning electron microscope after exposing them to 200 KV.

S2 Synthesis methodologies

S.2.1 N^1,N^1,N^4,N^4-Ttetrakis(4-bromophenyl)-p-phenylenediamine (TPPDA-4Br)

According to earlier reported work, the bromination of the pristine N^1,N^1,N^4,N^4-tetraphenyl-*p*-phenylenediamine (TPPDA) was achieved as briefed in Scheme S1. Briefly, the TPPDA (2.42 mmol, 1 g) and dry DMF (40 mL) were mixed into a 50 mL round bottom flask. After that, *N*-Bromosuccinimide (NBS) (10.8 mmol, 1.94 g) was solved in a 20 mL of dry DMF which then dropped wisely to the TPPDA solution at 0°C as well as gentle magnetic stirring overnight. Finally, the flask ingredients were poured onto icy water, and then filtered, rinsed sever times via ethanol (1.64 g, 93% yield). FTIR: 1576, 1499, 1016 cm^{-1} (Fig. S1). The ^{1}H-NMR ($CDCl_3$, 25 °C, 600 MHz): 7.35 (d, 8H), 6.94 (m, 12H). ^{13}C NMR ($CDCl_3$, 25 °C, 500 MHz): 132.3, 125.5, 125.2 ppm. *HRMS* (*ESI*): *m/z* calculated for $C_{30}H_{20}Br_4N_2$: 728.1; found 728.69 (Fig. S2).

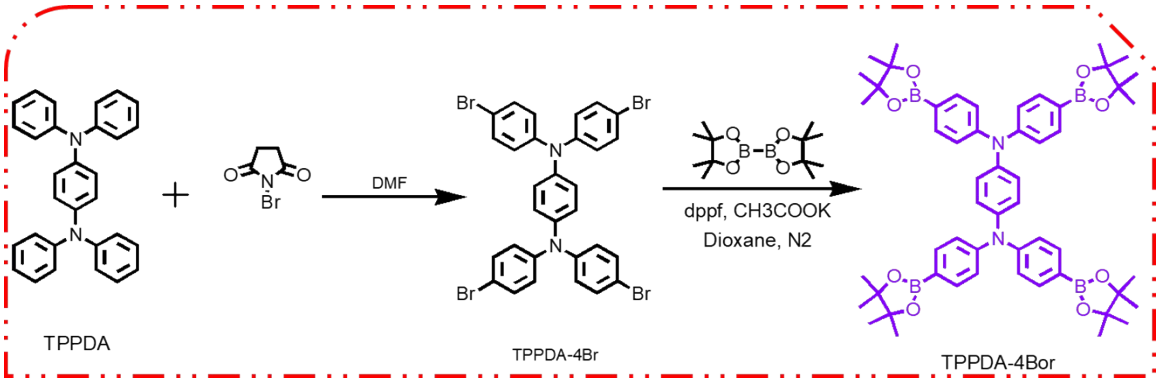

Scheme S1 Schematic synthesis of TPPDA, and TPPDA-4Bor

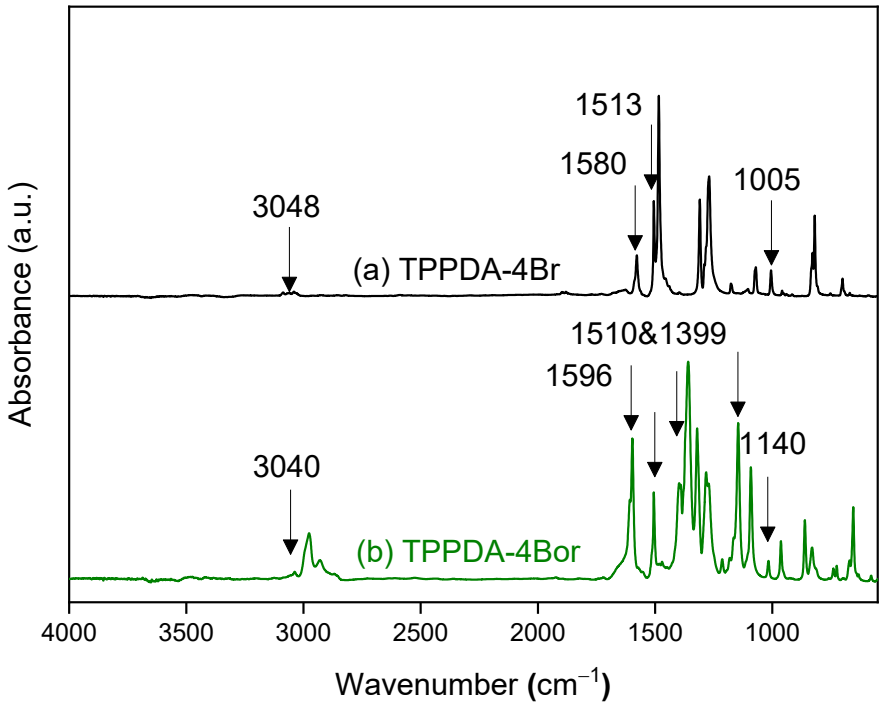

Fig. S1 FTIR of TPPDA-4Br, and TPPDA-4Bor

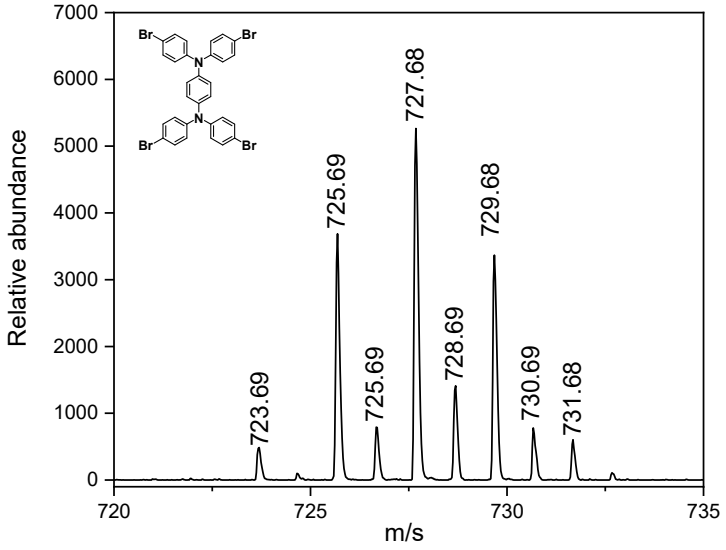

Fig. S2 Mass spectroscopy analysis of TPPDA-4Br

S.2.2 N^1,N^1,N^4,N^4-Tetrakis(4-(4,4,5,5-tetramethyl-1,3,2-dioxaborolan-2-yl)phenyl)-p-phenylene diamine (TPPDA-4Bor)

In a couple-neck flask, the previously designed TPPDA-4Br (1.2g, 5.8 mmol) was charged with the bis(pinacolato)diboron (2.6 g, 35.96 mmol), potassium acetate (0.5 g, 35,7 mmol), and 1,1′-ferrocenediyl-bis(diphenylphosphine) (dppf) (105 mg, 0.5 mmol) and then these powders were degassed for 15 min. Afterwards, a dioxane (50 mL) was charged to the flask under a nitrogenic pressure then the rection was kept at 110° C for 48 hours under refluxing conditions and stirring. Afterwards, the solution was poured onto icy water, then separated, rinsed, dried using ethanol as well. Column chromatography was applied ensuring the complete purging of the moiety via a co-solvent of THF and hexane of a ratio of 3:7. Notably, the precipitate was dried at 70° C (1.33 g, yield, 88 %). FTIR: 2976, 1503, 1392, 1268, 1144, 1015 cm^{-1} (Fig. S1). ^{1}H-NMR (DMSO, 25 °C, 600 MHz): 7.17 (d, J = 8.0 Hz, 8H), 7.06 (d, J = 8.0 Hz, 8H), and 6.96 (d, J = 8.0 Hz, 4H) (Fig. S3). ^{13}C-NMR (CDCl3, 25 °C, 500 MHz): 141.75, 133.25, 127.74, 121.78, 107.79, 83.92, 23.97 ppm (Fig. S4). HRMS: *m/z* calculated for $C_{54}H_{68}B_4N_2O_8$: 916.37; found 916.51 (Fig. S5).

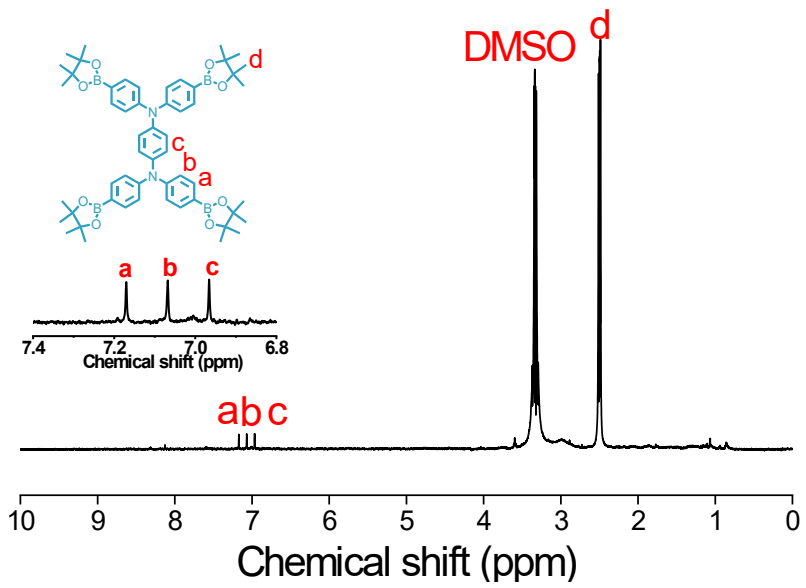

Fig. S3 ^{1}H NMR spectra of TPPDA-4Bor

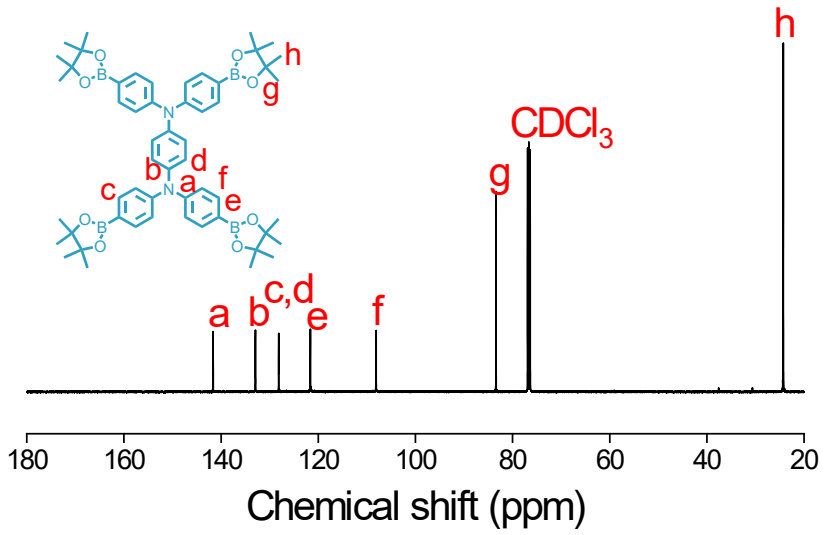

Fig. S4 ^{13}C NMR spectra of TPPDA-4Bor

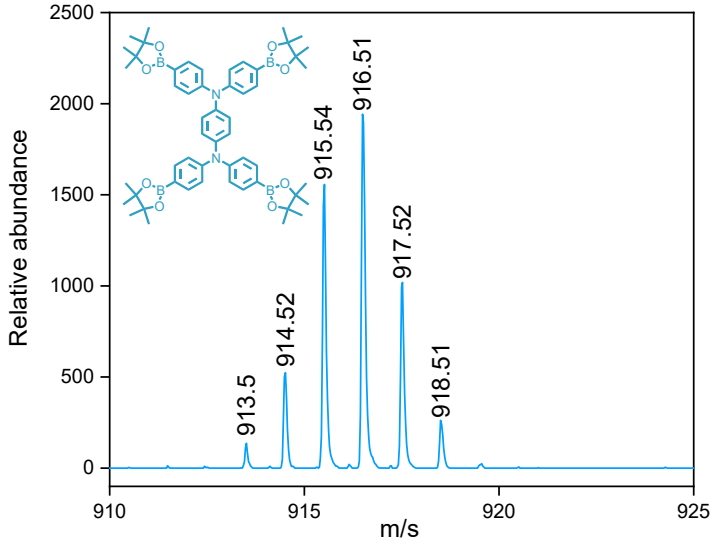

Fig. S5 Mass spectroscopy analysis of TPPDA-4Bor

S.2.3 Synthesis of Tris(4-bromophenyle)amine (TPA-3Br)

The TPA-3Br was designed and scanned according to the earlier work. Briefly, as clarified in scheme S2, a 250 mL flask was supplemented with triphenylamine (5 g, 4.08 mmol), DMF (120 mL) under icy and dark environment. A solution of NBS (12 g, 12.32 mmol), and DMF (60mL) was dropped wisely into the reaction flask under continuous magnetic stirring which lasted overnight at ambient temperature. After that, the yield was separated with dichloromethane (DCM) which then rinsed via methanol affording a white powder. FTIR scan: 3064, 1570, 1266, and 816 cm^{-1} (Fig. S6). ^{1}H NMR scan (400 MHz, 25 °C, CDCl3): δ 7.35 ppm (d, 6H), and 6.921 ppm (d, 6H) (Fig. S7). ^{13}C NMR scan ($CDCl_3$, 25 °C, 500 MHz): 146.7 ppm, 132.8, 126.01, and 116.38 ppm (Fig. S8).

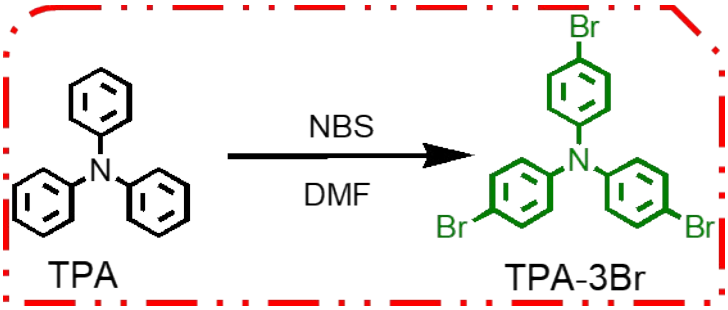

Scheme S2 Schematic design of TPA-3Br

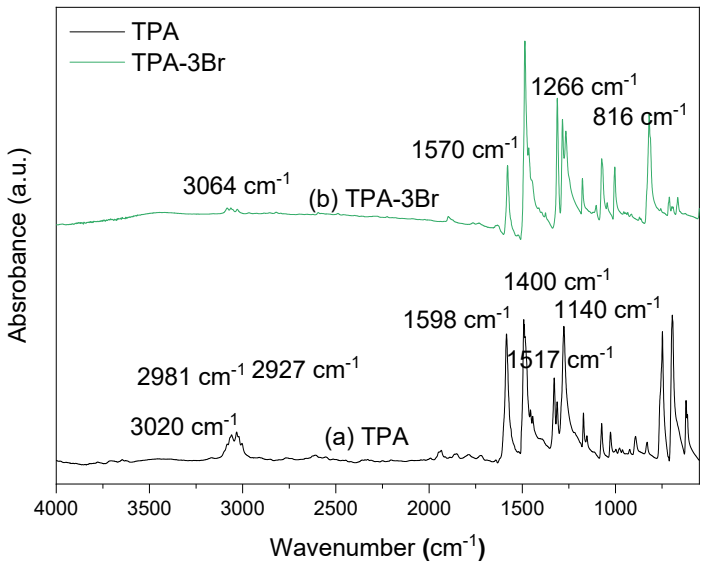

Fig. S6 FTIR of Pristine TPA, and TPA-3Br

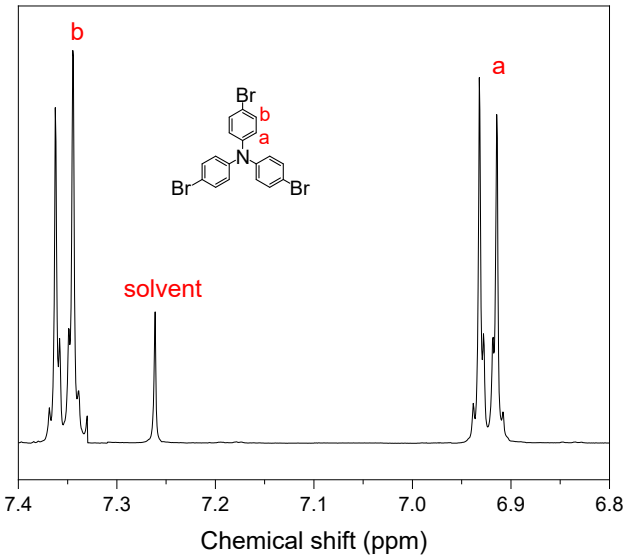

Fig. S7 ^{1}HNMR of TPA-3Br

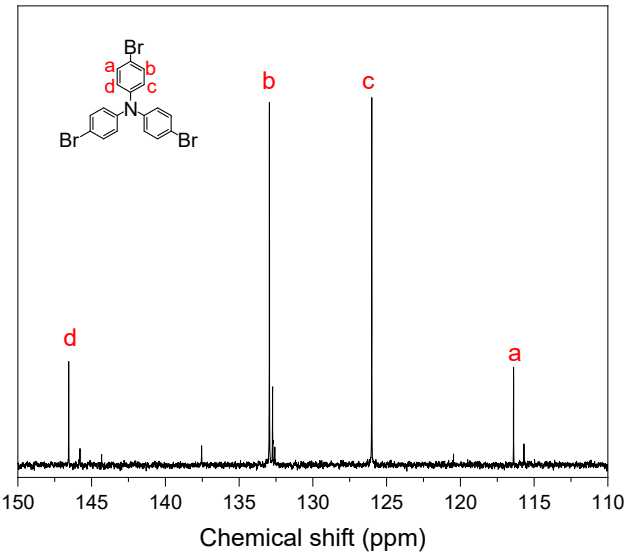

Fig. S8 ^{13}C NMR of TPA-3Br

S.2.1 Synthesis of 4,7-di(thiophen-2-yl)benzo[c][1,2,5]thiadiazole (ThZ)

The 4,7-di(thiophen-2-yl)benzo[c][1,2,5]thiadiazole (ThZ) was designed via following the reported study as schemes briefly in Scheme S3. The commercial 4,7-Dibromo-2,1,3-

benzothiadiazole (Tz-2Br) (750 mg, 2.551 mmol) with tetrakis(triphenylphosphine) palladium(0) (590 mg, 0.510 mmol) were intermixed in a round flask which then degassed for 15 min. Afterwards, the reaction was continued after the injection of dry *N*,*N*-Dimethylformamide (DMF, 10 mL) and 2-(tributylstannyl)thiophene (2.43 mL) under N_2 atmosphere. The flask was refluxed for 72 h at 120 °C under N_2 atmosphere under continues magnetic stirring. Finally, an orange precipitate was formed after solvent evaporation. The powder was finally purified employing the column chromatography via eluent of DCM/hexane (1:4 *v*/*v*). FTIR (KBr pellets): 2965, 1730, 1633, and 1261 cm^{-1} (Fig. S9). ^{1}H NMR (400 MHz, 25 °C): δ = 8.13 (*d*, 2H), 7.88 (*s*, 2H), 7.47 (*d*, 2H) and 7.20 (*m*, 2H) ppm (Fig. S10). The melting point was recorded as 120-122 °C.

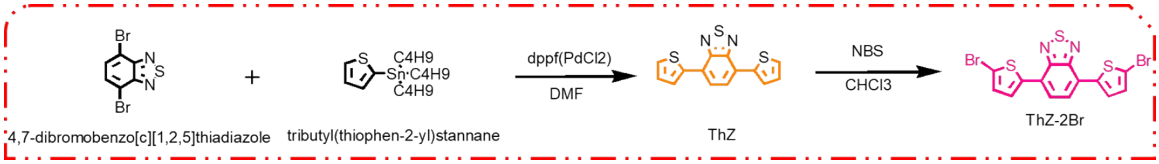

Scheme S3 Schematic design of ThZ, and ThZ-2Br.

S.2.2 Synthesis of 4,7-bis(5-bromothiophen-2-yl)benzo[c][1,2,5]thiadiazole (ThZ-2Br)

According to the previous report,[1] 4,7-bis(5-bromothiophen-2-yl)benzo[c][1,2,5]thiadiazole (ThZ-2Br) was also designed employing the above synthesized ThZ (637 mg, 2.12 mmol) after dissolving it into a 50 mL chloroform which then mixed with *N*-bromosuccinimide (831 mg) in a couple-neck flask in dark environment. The reaction was conducted in the dark, under N_2 stream, and at an ambient temperature for 3 nights. Finally, the powder was separated, rinsed as well with water, methanol, and chloroform. The yielded red powder was dried under vacuum overnight. ^{1}H NMR (400 MHz, 25 °C): δ = 7.82 (*d*, 2H), 7.81 (*s*, 2H), and 7.17 (*d*, 2H) ppm (Fig. S11). The melting point was recorded to be 252-254 °C.

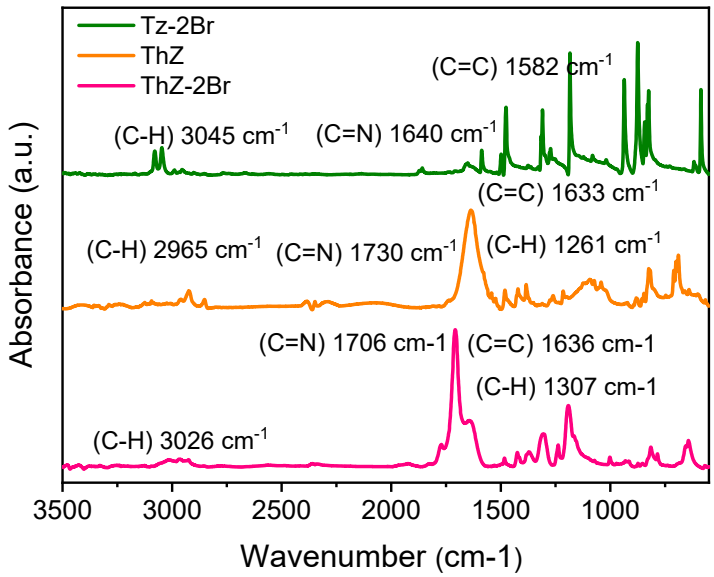

Fig. S9 FTIR of pristine Tz-2Br, ThZ, and ThZ-2Br

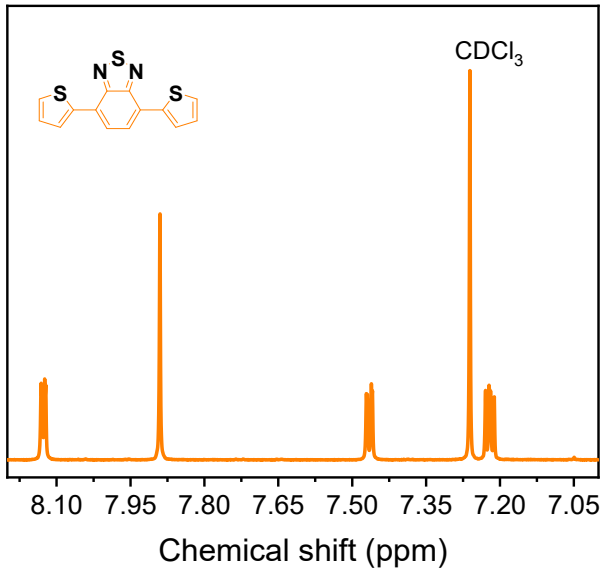

Fig. S10 ^{1}HNMR of the ThZ

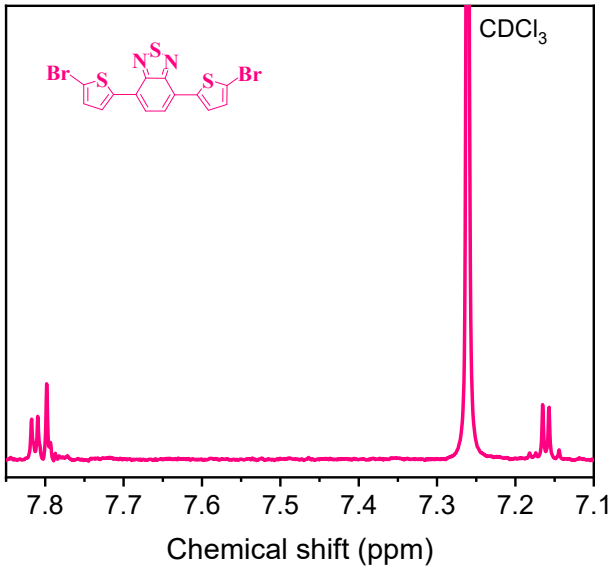

Fig. S11 1HNMR of the ThZ-2Br

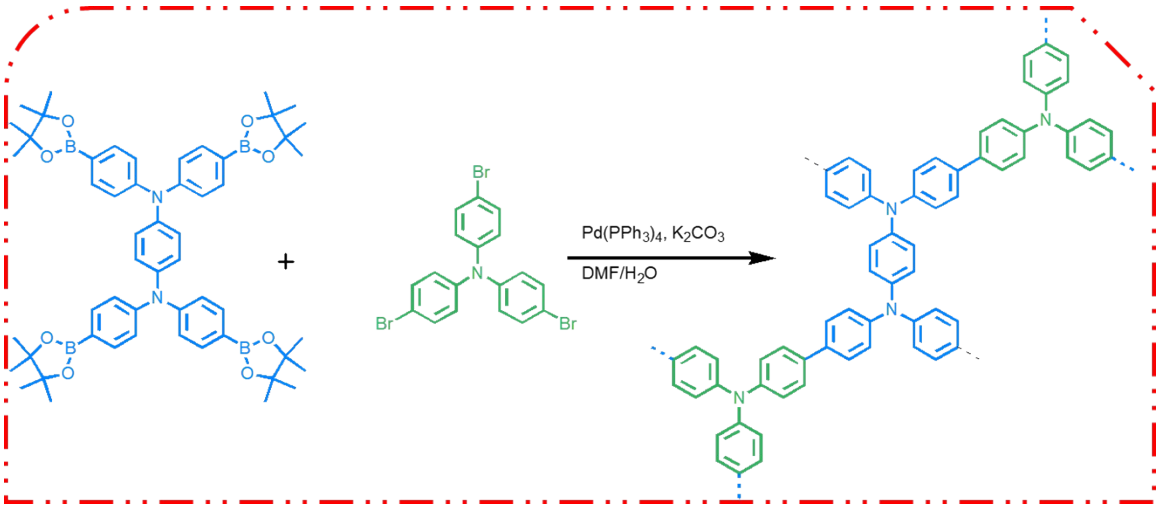

Scheme S4 Synthesis design of TPPDA-TPA CMP

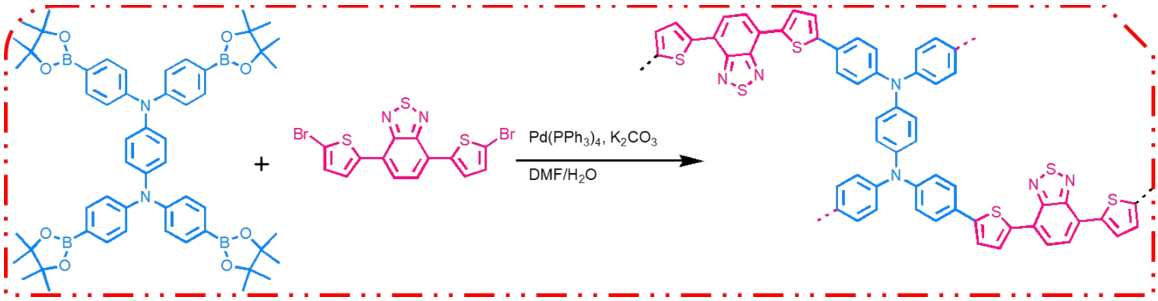

Scheme S5 Schematic design of TPPDA-ThZ CMP

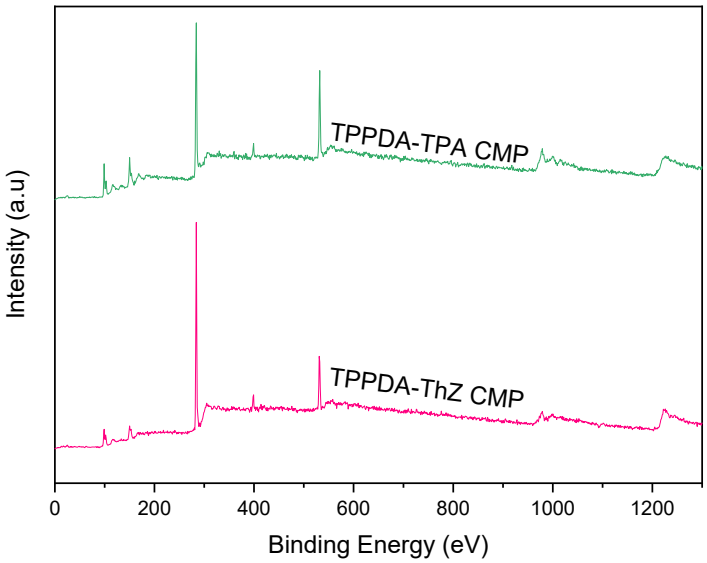

Fig. S12 Wide-scan XPS of TPPDA-TPA, and TPPDA-ThZ CMPs

Table S1 XPS fitting properties of TPPDA-TPA, and TPPDA-ThZ CMPs.

Element	**Status**	**Binding Energy (eV)**	**TPPDA-TPA CMP**		**TPPDA-ThZ CMP**	
			FWHM	Area	FWHM	Area
C1s	C=C	283.698	1.4	7476.945	0.93	5368.317
	C=N	284.188	1.69	751.6447	0.84	4390.3
	C-OH	284.75	1.58	2223.07	1.12	1701.041
	C=O or C-S	287.5399	3.96	687.568	0.86	224.93
N1s	N-C	398	1.34	642.4345	1.377	187.38
	N-S	398.136			0.95	332.86
	N_2	399.1	1.3	128.6982	1.63	282.2966
O1S	O-S	530.99			1.73	1823.45
	O=C	531.6	1.42	2511.272	1.335	1621.45
	C-OH	532.399	1.71	3764.766	1.15	732.12
S2p	C-S	163.399			3.82	81.685
	$S2p_{3/2}$	164.9			3.0778	211.22
	S-O	167.699			2.8	353.699
	S2P1/2	168.799			3.88	193.565

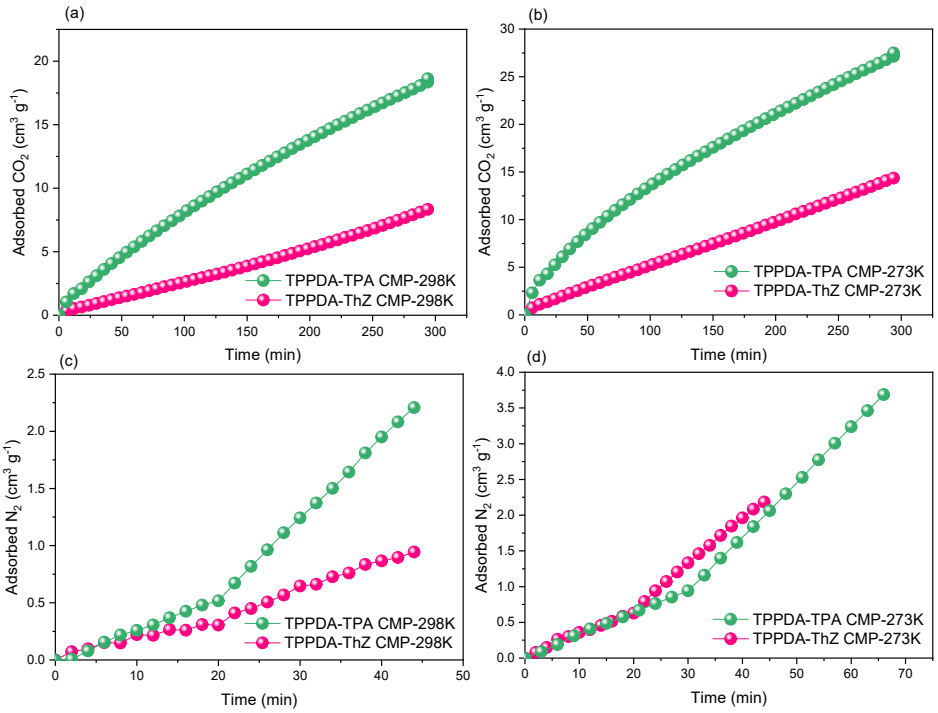

Fig. S 13 Time dependent relationships of CO_2 (a, b), and N_2 (a, b) uptake onto TPPDA-TPA, and TPPDA-ThZ CMPs at 298 K, and 273 K.

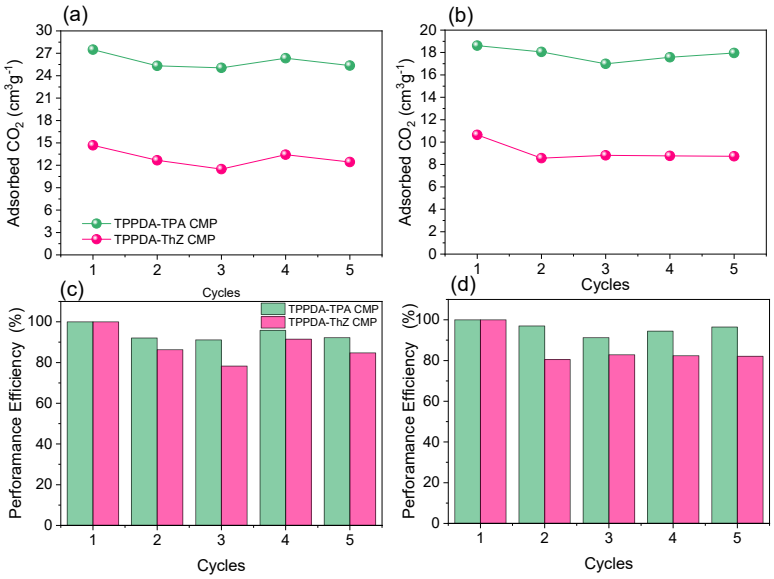

Fig. S 14 Adsorption capacities of CO2 utilizing those TPPDA-TPA, and TPPDA-ThZ CMP at 273 K (a) and 298 K (b) respectively over five runs. Performance Efficiency of TPPDA-TPA, and TPPDA-ThZ CMP at 273 K (c) and 298 K (d) respectively.

Table S2 The CO2, N2 uptakes, selectivity, and isosteric heats at various pressures using TPPDA-TPA, and TPPDA-ThZ CMPs

Sample	CO_2 uptake (cm^3g^{-1})		N_2 uptake (cm^3g^{-1})		Selectivity CO_2/N_2		Qst of CO_2 uptake (KJ mol^{-1})		Qst of N_2 uptake (KJ mol^{-1})	
	273 K	298 K	273 K	298 K	273 K	298 K	0.1 bar	0.4 bar	0.005 bar	0.04 bar
TPPDA-TPA CMP	27.49	18.6	3.686	2.207	7.47	8.433	24.04	20.44	26.7	15.39
TPPDA-ThZ CMP	14.67	8.81	2.184	0.944	6.72	9.333	23.26	13.75	10.34	27.67

Table S3 Comparative study of TPPDA-TPA, and TPPDA-ThZ CMPs for CO2 adsorption with earlier reported porous materials.

Sample	**CO_2 uptake (mmol/g)**		**Ref.**
	273 K	298 K	
RLF-500	3.13	--	[2]
ELF6	3.29	--	[3]
ELF46	2.46	--	[3]
PECONF-1	1.86	1.34	[4]
PECONF-2	2.85	1.98	[4]
PECONF-4	2.95	1.96	[4]
BPOP-1	1.79	0.98	[5]
BPOP-2	1.45	0.67	[5]
COF-102	1.56	--	[6]
Fc-CMP-1	1.45	--	[7]
BoxPOP-1	--	0.91	[8]
BoxPOP-2	--	1.04	[8]
BoxPOP-3	--	0.29	[8]
$Co_3(BTB)_2(DMA)_4$	--	0.678	[9]
PP1-2-TAEA	1.13	--	[10]
CHIT	--	0.1	[11]
CHIT-HTC-12	--	0.1	[11]
CHIT-HTC-24	--	0.3	[11]
CHIT-HTC-48	--	0.45	[11]
BGM	--	0.247	[12]

BGM2	--	0.252	[12]
BGM6	--	0.295	[12]
BGM10	--	0.581	[12]
ISM-1	--	5 (mg g^{-1})	[13]
ISM-5	--	9.3 (mg g^{-1})	[13]
AlPor–PIP–Br	1.3	--	[14]
PE-SBA-15	--	0.27	[15]
TPPDA-TPA CMP	1.27	0.83	This study
TPPDA-ThZ CMP	0.65	0.39	

S3 References

1 M. G. Kotp, N. L. Torad, H. Nara, W. Chaikittisilp, J. You, Y. Yamauchi, A. F. M. El-Mahdy and S.-W. Kuo, Tunable Thiophene-Based Conjugated Microporous Polymers for the Disposal of Toxic Hexavalent Chromium, *J. Mater. Chem. A*, 2023, **11**, 15022-15032.

2 G. P. Hao, W. C. Li, D. Qian and A. H. Lu, Rapid synthesis of nitrogen-doped porous carbon monolith for CO2 capture, *Adv. Mater.*, 2010, **22**, 853-857.

3 W. Shi, X. Zhang, Y. Ji, Z. Zhao, W. Li and X. Jia, Sustainable preparation of bio-based polybenzoxazine resins from amino acid and their application in CO2 adsorption, *ACS Sustain. Chem. Eng. ACS*, 2019, **7**, 17313-17324.

4 P. Mohanty, L. D. Kull and K. Landskron, Porous covalent electron-rich organonitridic frameworks as highly selective sorbents for methane and carbon dioxide, *Nat. Commun*, 2011, **2**, 401.

5 X. Sun, J. Li, W. Wang and Q. Ma, Constructing benzoxazine-containing porous organic polymers for carbon dioxide and hydrogen sorption, *Eur. Polym. J.*, 2018, **107**, 89-95.

6 H. Furukawa and O. M. Yaghi, Storage of hydrogen, methane, and carbon dioxide in highly porous covalent organic frameworks for clean energy applications, *J. Am. Chem. Soc.*, 2009, **131**, 8875-8883.

7 G. Li, Q. Liu, B. Liao, L. Chen, H. Zhou, Z. Zhou, B. Xia, J. Huang and B. Liu, Synthesis of novel ferrocene-based conjugated microporous polymers with intrinsic magnetism, *Eur. Polym. J.*, 2017, **93**, 556-560.

8 S. Xu, J. He, S. Jin and B. Tan, Heteroatom-rich porous organic polymers constructed by benzoxazine linkage with high carbon dioxide adsorption affinity, *J. Colloid Interface Sci.*, 2018, **509**, 457-462.

9 D. Kim, X. Song, J. H. Yoon and M. S. Lah, 3, 6-Connected metal–organic frameworks based on triscarboxylate as a 3-connected organic node and a linear trinuclear Co3 (COO) 6 secondary building unit as a 6-connected node, *Cryst. Growth Des.*, 2012, **12**, 4186-4193.
10 T. Shi, Z. Wu, Z. Wu, Q. F. Zhang, M. Strømme and C. Xu, Postsynthetic amine modification of porous organic polymers for CO2 capture and separation, *Journal of Polymer Science*, 2024, **62**, 1554-1568.
11 J. A. Chagas, G. O. Crispim, B. P. Pinto, R. A. San Gil and C. J. Mota, Synthesis, characterization, and CO2 uptake of adsorbents prepared by hydrothermal carbonization of chitosan, *ACS omega*, 2020, **5**, 29520-29529.
12 M. Mirković, M. S. Yilmaz, L. Kljajević, V. Pavlović, M. Ivanović, D. Djukić and T. Eren, Design of PEI and amine modified metakaolin-brushite hybrid polymeric composite materials for CO2 capturing, *Polymers*, 2023, **15**, 1669.
13 K. Cai, P. Liu, Z. Chen, P. Chen, F. Liu, T. Zhao and D.-J. Tao, Construction of bifunctional triazine-based imidazolium porous ionomer polymers by a post-crosslinking tactic for efficient CO2 capture and conversion, *Chem. Eng. J.*, 2023, **451**, 138946.
14 X. Liu, Y. Yang, M. Chen, W. Xu, K. Chen and R. Luo, High-surface-area metalloporphyrin-based porous ionic polymers by the direct condensation strategy for enhanced CO2 capture and catalytic conversion into cyclic carbonates, *ACS Appl. Mater. Interfaces*, 2022, **15**, 1085-1096.
15 A. A. Al-Absi, A. Domin, M. Mohamedali, A. M. Benneker and N. Mahinpey, CO2 capture using in-situ polymerized amines into pore-expanded-SBA-15: Performance evaluation, kinetics, and adsorption isotherms, *Fuel*, 2023, **333**, 126401.